Eur. Phys. J. D **17**, 113–123 (2001)

THE EUROPEAN PHYSICAL JOURNAL D

EDP Sciences

Coherent population trapping involving Rydberg states in xenon probed by ionization suppression

T. Halfmann[a], K. Böhmer, L.P. Yatsenko[b], A. Horsmans, and K. Bergmann

Fachbereich Physik der Universität, Universität Kaiserslautern, 67663 Kaiserslautern, Germany

Received 7 May 2000 and Received in final form 25 June 2001

Abstract. We report the observation of pronounced coherent population trapping and dark resonances in Rydberg states of xenon. A weak two-photon coupling with radiation of $\lambda_P = 250$ nm is induced between the $5p^6\ ^1S_0$ ground state of xenon and state $5p^5 6p[1/2]_0$, leading to (2+1) resonantly enhanced three-photon ionization. The state $5p^5 6p[1/2]_0$ is strongly coupled by radiation with $\lambda_D \simeq 600$ nm to $5p^5 ns[J_C]_1$ or $5p^5 nd[J_C]_1$ Rydberg states with principal quantum numbers n in the range $18 \leq n \leq 23$ and with the rotational quantum number of the ionic core $J_C = 1/2$ or $J_C = 3/2$. The ionization is monitored through observation of the photoelectrons with an energy resolution $\Delta E = 150$ meV which is sufficient to distinguish the ionization processes into the two ionization continua. Pronounced and robust dark resonances are observed in the ionization rate whenever λ_D is tuned to resonance with one of the ns- or nd-Rydberg states. The dark resonances are due to efficient population trapping in the atomic ground state $5p^6\ ^1S_0$ through the suppression of excitation of the intermediate state $5p^5 6p[1/2]_0$. The resolution is sufficient to resolve the hyperfine structure of the ns-Rydberg levels for odd xenon isotopes. The hyperfine splitting does not vary significantly with n in the given range. Results from model calculations taking the natural isotope abundance into account are in good agreement with the observed spectral structures. Pronounced dark resonances are also observed when the dressing radiation field with λ_D is generated from a laser with poor coherence properties. The maximum reduction of the ionization signal clearly exceeds 50%, a value which is expected to be the maximum, when the dip is caused by saturation of the transition rate between the intermediate and the Rydberg state due to incoherent radiation. This work demonstrates the potential of dark resonance spectroscopy of high lying electronic states of rare gas atoms.

PACS. 42.50.Hz Strong-field excitation of optical transitions in quantum systems; multi-photon processes; dynamic Stark shift – 32.80.Rm Multiphoton ionization and excitation to highly excited states (*e.g.*, Rydberg states) – 32.10.Fn Fine and hyperfine structure

1 Introduction

The interaction of strong, coherent radiation with matter permits the manipulation of atomic and molecular systems and processes beyond the limits imposed by incoherent excitation. Examples of processes that rely on coherent interactions are population transfer by Rapid Adiabatic Passage (RAP) [1,2], Stimulated Raman Scattering involving Adiabatic Passage (STIRAP) [3], Stark-Chirped Rapid Adiabatic Passage (SCRAP) [4], Electromagnetically Induced Transparency (EIT) in otherwise opaque media [5,6], Coherent Population Trapping (CPT) and dark resonances [7] in radiative decay or fragmentation processes [8,9] as well as coherent control of these processes [10].

A typical example for a spectroscopic technique which relies on coherence is the preparation of dark resonances in a lambda-type or ladder-type level scheme [7,11,12]. A populated ground or metastable state is weakly coupled to an excited intermediate state by a probe laser field. The intermediate state is coupled to a target state by a strong dressing laser field. When the dressing laser is switched on, the transfer of population from the ground to the intermediate state by the probe laser is inhibited as in EIT. Unlike for STIRAP, where *both* radiation fields induce strong couplings, the population is trapped in the ground state rather than being transferred to the Rydberg state, without placing transient population into the intermediate level.

The population of the intermediate state may be probed by observing decay channels such as fluorescence, (pre-) dissociation or ionization. A reduction of the intermediate state population of up to 50% may also be caused by saturation, if an incoherent radiation field is strong enough to equilibrate the population between the

[a] e-mail: halfmann@physik.uni-kl.de

[b] *Permanent address:* Institute of Physics, Ukrainian Academy of Sciences, prospekt Nauki 46, Kiev-22, 252650, Ukraine.

intermediate and the target state. Such a process is the basis of the very successful method of stimulated emission pumping [15].

When the transitions are driven by radiation with transform-limited bandwidth and the Rabi frequency $\Omega = \mu E/\hbar$ (μ is the transition dipole moment and E is the electric field of the radiation) which describes the strength of the interaction, is larger than other competing rates (like the rate of radiative decay) the dressed state formalism is appropriate to describe the process. In the dressed state picture the weak probe laser couples the ground state to a pair of levels, separated by the Autler-Townes splitting [1], which is equal to the Rabi frequency related to the dressing laser induced coupling. The coherent nature of that interaction results in a cancellation of the effective transition dipole moment, when the probe laser frequency is tuned exactly to resonance with the transition frequency between the ground and the intermediate bare state. The cancellation of the transition dipole moment is the basis of EIT [6]. Population transfer from the ground state to the excited state is no more possible. A dark resonance, *i.e.* a suppression of decay processes from the excited state is observed. In fact, the formation of dark resonances is the basis of coherent fluorescence dip spectroscopy (CFS) [7] or coherent ion dip spectroscopy (CIS) [11] of atomic and molecular systems.

Dark resonance spectroscopy involving one-photon transitions only does not permit the study of highly excited states, such as Rydberg states without the need of vacuum-ultraviolet radiation with photon energy in the range from 10–20 eV. Such radiation is available from synchrotrons or by frequency conversion techniques, like four-wave mixing or high-order harmonic generation. In general, the efficiency of these frequency conversion techniques does not exceeds 10^{-4}. In this publication we extend the technique of dark resonance spectroscopy to a ladder-system involving multi-photon excitations, permitting the investigation of highly excited states with ultraviolet and visible radiation, provided by either a narrow- or a broadband laser-system. Figure 1 shows the coupling scheme, used in this work. A weak two-photon coupling with radiation of $\lambda_{\mathrm{P}} = 250$ nm is induced between the $5p^6\ {}^1\mathrm{S}_0$ ground state of xenon and the intermediate state $5p^5 6p[1/2]_0$, leading to (2+1) resonantly enhanced multi-photon ionization. The intermediate state is strongly coupled by radiation with $\lambda_{\mathrm{D}} \approx 600$ nm to $5p^5 ns[J_{\mathrm{C}}]_1$ or $5p^5 nd[J_{\mathrm{C}}]_1$ Rydberg states with principal quantum numbers n in the range $18 \leq n \leq 23$ and with the rotational quantum number of the ionic core $J_{\mathrm{C}} = 1/2$ or 3/2. The ionization, as a probe for the population distribution in the atomic system, is monitored through the observation of photoelectrons with an energy resolution of $\Delta E = 150$ meV, which is sufficient to distinguish ionization processes into the two ionization continua. The coupling scheme described here is closely related to experiments on four-wave mixing enhanced by electromagnetically induced transparency [6]. The role of Rydberg states in such frequency conversion processes has been investigated by Zhang *et al.* [16].

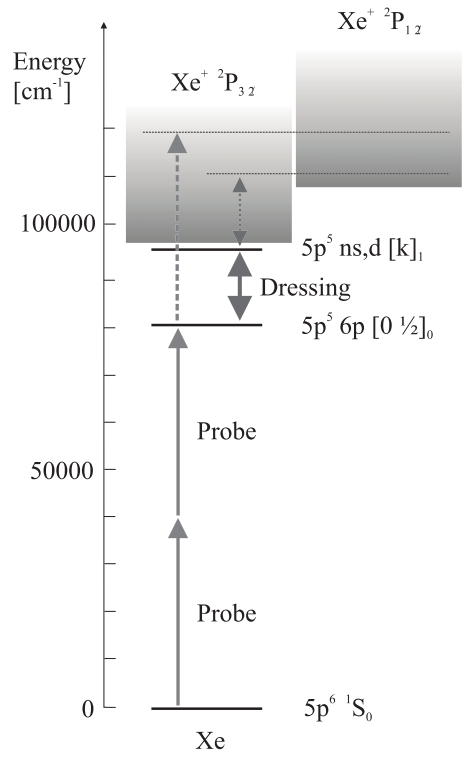

Fig. 1. Excitation scheme: the xenon atoms are excited by the weak probe laser from the ground state $5p^6\ {}^1\mathrm{S}_0$ to the excited state $5p^5\ 6p[1/2]_0$ in a two-photon transition. Another photon of the same energy serves to ionize the xenon atoms. The excited state $5p^5\ 6p[1/2]_0$ is coupled by the strong dressing laser to highly excited Rydberg states. In a competing process the dressing laser may transfer population to the excited Rydberg state and subsequently ionize the atom. The detection of the photoelectrons with kinetic energy resolution permits selective observation of the different ionization channels.

An alternative well known detection scheme in Rydberg state spectroscopy employs field ionization of the Rydberg levels, which are populated *via* either single-photon or multi-photon transitions [17]. Although that scheme is suitable for very high resolution studies if continuous lasers can be used, it is limited to the study of states very close to the ionization limit. The dark resonance spectroscopy via intermediate state ionization, as employed here, may suffer from laser-induced Stark shifts [1,18–20], unless two-photon excitation of the intermediate state occurs exactly on resonance, but it is applicable to any electronically excited state.

2 Experimental setup

Xenon gas with natural isotope abundance is expanded from a stagnation region at room temperature and a pressure of typically 500 mbar through a pulsed nozzle (General Valve, opening diameter 0.8 mm). The resulting supersonic jet is collimated by a skimmer (orifice 0.8 mm), 132 mm downstream from the nozzle. The skimmer separates the source chamber from the interaction

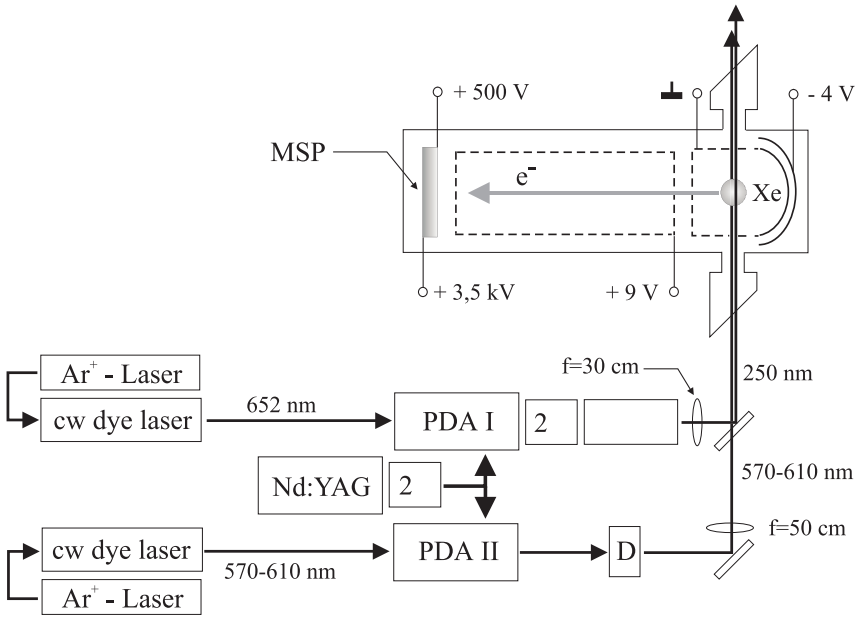

Fig. 2. The experimental setup with a laser-system providing pulses of transform-limited bandwidth: the $5p^6\,{}^1S_0$–$5p^5\,6p[1/2]_0$ – transition in xenon, is excited by radiation at 250 nm, which is generated by frequency conversion (frequency doubling and sum-frequency mixing) of the output from a pulsed dye amplifier, seeded by a tunable single-mode cw laser-system. The output of a second pulsed dye amplifier, operated with appropriate laser dyes, provides the dressing laser pulse, tunable in the range 570–610 nm. After the dressing laser pulse has passed an optical delay line (D), both lasers are focussed into the atomic jet. The photoelectrons generated in the excitation process are collected by an electrostatic parabolic mirror and, after passing through a time-of-flight segment (length $l = 1$ m), detected on a micro-sphere plate. The energy resolution of the setup was typically 150 meV.

and detection region. The pulsed beam of xenon atoms is intersected at right angle by the lasers at a distance of 103 mm downstream from the skimmer. The particle density in the interaction region is estimated to be approximately 10^{13} atoms/cm^3.

The photoelectrons from the ionization of the intermediate state are detected in an electron spectrometer, consisting of a parabolic electrostatic mirror, the focus of which coincides with the interaction region. The electrons are accelerated and, after passing through a time-of-flight segment, detected on a micro-sphere-plate (El Mul Technologies). The signal output of the micro-sphere-plate is amplified by fast broadband amplifiers and processed in boxcar gated integrators (EG&G 4121B). The energy resolution of the spectrometer is typically $\Delta E = 150$ meV, which is sufficient to resolve photoelectrons from the two ionization continua of xenon. In the experiments discussed here, the photoelectrons from all the possible one- and multi-photon ionization processes (see Fig. 1) can be distinguished.

Coherent radiation with transform-limited bandwidth is provided by pulsed amplification of single-mode cw radiation (see Fig. 2). The probe laser pulse is provided by a pulsed dye amplifier (Quanta Ray PDA), seeded by the output of a single-mode cw dye laser (Coherent 699) operating at 652 nm. The amplifier is pumped by the frequency doubled radiation of an injection seeded pulsed Nd:YAG laser (Quanta Ray GCR 4). The output of the pulsed dye amplifier is frequency doubled in a BBO crystal and mixed with the fundamental frequency of the Nd:YAG laser in a KDP crystal to obtain radiation at 250 nm with pulse energies up to a few 100 μJ and a pulse duration of $\tau_P = 3.4$ ns (FWHM of the intensity). The spectral bandwidth of the ultraviolet radiation is about $\Delta\nu = 140$ MHz, which is very close to the transform limit $\Delta\nu_{\min} = 130$ MHz for laser pulses with a Gaussian temporal profile. A second pulsed dye amplifier, seeded by another cw dye laser-system running at 570–610 nm with a modehop free tuning range of 20 GHz, provides the dressing laser pulse with pulse energies up to several mJ and a pulse duration of $\tau_D = 5.5$ ns (FWHM of the intensity). The dressing laser pulse passes through an optical delay line before it is spatially overlapped with the probe laser beam axis. The temporal overlap of the two laser pulses is controlled by adjusting the length of the delay line. The laser beams are focussed by quartz lenses onto the axis of the atomic beam. The beam diameters (FWHM of intensity) in the interaction region were 170 μm for the probe and 670 μm for the dressing laser, yielding peak intensities up to 160 MW/cm^2 for the probe and 220 MW/cm^2 for the dressing laser. The probe laser was attenuated to intensities typically in the range of a few MW/cm^2 in order to prevent saturation of the electron detection. At these intensities the probe laser-induced transition is far from being saturated, therefore it does not affect the coherent coupling induced by the dressing laser (see below).

Alternatively we used two dye lasers (LPD3000), pumped by an excimer laser (LPX 220i) to provide

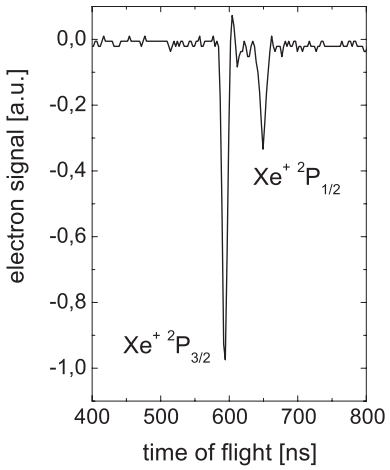

Fig. 3. Electron energy spectrum obtained after (2+1) resonantly enhanced multi-photon ionization of population from the ground state $5p^6\,{}^1\mathrm{S}_0$ in xenon *via* the intermediate state $5p^5\,6p[1/2]_0$ with the probe laser operating at $\lambda_\mathrm{P} = 250$ nm. The dressing laser was switched off. The fine structure components $2\mathrm{P}_{3/2}$ and $2\mathrm{P}_{1/2}$ of the xenon ion are clearly resolved in the electron spectrum.

broadly tunable radiation with a bandwidth of 6 GHz and pulse duration of about 15 ns. The radiation of one of the dye lasers was frequency doubled in BBO to obtain the ultraviolet radiation for the probe laser pulse. The maximum intensity provided by this laser-system was comparable to that one from the system with nearly transform-limited spectral bandwidth. However, due to the larger bandwidth, the spectral intensity was about two orders of magnitude smaller.

Figure 3 shows an example of an electron energy spectrum with the dressing laser switched off. The two groups of electrons with different energy relate to the ionization into the two continua, leaving the ionic core either in the $J_\mathrm{C} = 1/2$ or in the $J_\mathrm{C} = 3/2$ fine structure state. The dark resonances are detected by observing any one of these ionization channels as the dressing laser is tuned across the resonance between the intermediate state $5p^5\,6p[1/2]_0$ and a Rydberg state. The transitions are assigned based on spectroscopic data given in [21,22]. On resonance, the electron intensity is reduced to nearly zero. Electrons with an energy corresponding to the ionization of Rydberg states by any of the two lasers were not observed.

3 Results

We discuss the results in three subsection. In Section 3.1, we present all observed dark resonances and offer some general comments. Section 3.2 deals with the specific case of the coupling to ns-Rydberg levels. The hyperfine structure of those states is revealed in the dark-resonance spectrum in a non-trivial way. Finally we demonstrate in Section 3.3 that dark resonances can also be observed when using the spectrally rather broad radiation from an excimer-pumped dye laser-system.

3.1 Dark resonances spectra

Figure 4 shows the recorded dark resonances. Nearly complete suppression of ionization, *i.e.* suppressed excitation of the intermediate state $5p^5\,6p[1/2]_0$ was found for dressing laser intensities exceeding 2 MW/cm^2, when the laser frequency was tuned to $nd[3/2]_1$ Rydberg states, and about 15 MW/cm^2 when tuned to $nd[1/2]_1$ or $ns[3/2]_1$ Rydberg states. The electron spectrum does not reveal any feature belonging to the possible ionization of population in the Rydberg states by the strong dressing laser. This confirms that all population is trapped in the atomic ground state, as expected. In fact, the Rabi frequency related to the coupling induced by the dressing laser is much larger than the Rabi frequency related to the two-photon coupling induced by the probe laser. Since this is true throughout the interaction the population remains trapped in the ground state [12,23].

For higher dressing laser intensity, power broadening of the dark resonances up to several 10 GHz was observed, thus indicating strong interaction. Detuning of the probe laser frequency from the two-photon resonance between the states $5p^6\,{}^1\mathrm{S}_0$ and $5p^5\,6p[1/2]_0$ lead to an asymmetric shape of the dark resonance (see Fig. 5).

Recording the photoelectrons, which belong to the two ionization continua, while the dressing laser couples the intermediate state to a given Rydberg state leads, as expected, to dark resonances with similar line shape. As also expected, dark resonances were observed, when the dressing laser was delayed with respect to the probe laser. However, the dressing laser pulse intensity, which was necessary to achieve complete population trapping, increased with the pulse delay, because the probe laser acted in the wings of the dressing laser pulse.

3.2 Effect of hyperfine structure on dark resonances

Is is apparent from Figure 4 that the coupling of the dressing laser to ns-Rydberg states leads to a peak near the center of the dark resonance. The relation of this structure to the hyperfine splitting of the Rydberg levels will be discussed in this section.

There are nine stable xenon isotopes in natural abundance: ^{124}Xe (0.0096%), ^{126}Xe (0.0090%), ^{128}Xe (1.92%), ^{129}Xe (26.4%), ^{130}Xe (4.1%), ^{131}Xe (21.1%), ^{132}Xe (26.9%), ^{134}Xe (10.4%), ^{136}Xe (8.9%). The isotope shift for xenon ($Z = 54$) is relatively small (a few hundred MHz) [24]. The nuclear spin of even xenon isotopes is $I = 0$. The ^{129}Xe isotope has $I = 1/2$ and ^{131}Xe has $I = 3/2$. As a result 47.5% of the xenon atoms show hyperfine structure. For ^{129}Xe each level with $J \neq 0$ is a doublet with splitting $\Delta_{(F,F-1)} = AF$, where A is the magnetic dipole constant. For ^{131}Xe the frequency differences between the HFS components is given by

$$\Delta_{(F,F-1)} = AF + \frac{3}{2}BF\left(\frac{F^2+\frac{1}{2}-J(J+1)-I(I+1)}{IJ(2J-1)(2I-1)}\right). \quad (1)$$

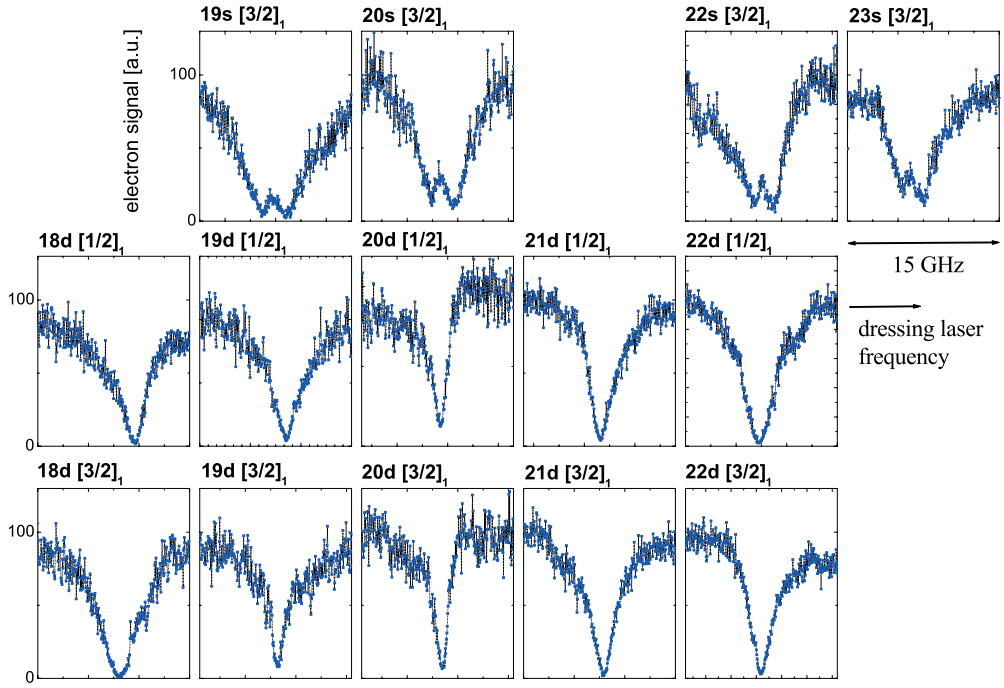

Fig. 4. Dark resonances in the photoionization of state $5p_5\,6p[1/2]_0$, when the dressing laser is tuned across the resonance between state $5p^5\,6p[1/2]_0$ and a Rydberg state. The tuning range of the dressing laser in all plots is 15 GHz. Complete suppression of the population of state $5p^5 6p[1/2]_0$ is observed for the coupling to 16 Rydberg states. About 2 MW/cm^2 were used for coupling to Rydberg states $nd[3/2]_1$ and about 15 MW/cm^2 for Rydberg states $nd[1/2]_1$ or $ns[3/2]_1$. We confirmed, that the structure of the dark resonance is the same in both ionization channels of xenon. For simplicity we show only the electron signal, corresponding to the lower continuum. No photoelectrons corresponding to ionization out of the Rydberg states with the dressing laser were found. From this we conclude that the total population of the system was trapped in the ground state $5p^6\,{}^1\mathrm{S}_0$. Due to hyperfine splitting for odd xenon isotopes, the dark resonances for the $ns[3/2]_1$ states reveal a peak near their centers (see Fig. 7).

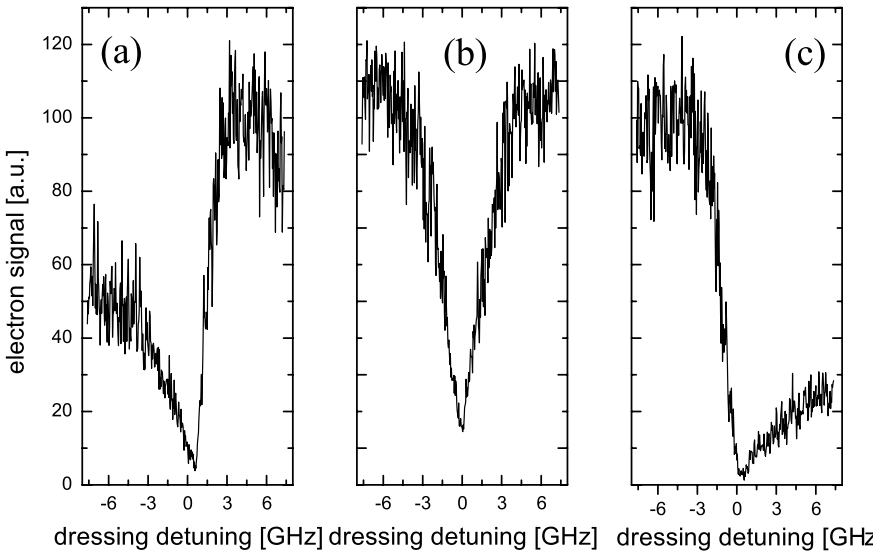

Fig. 5. Dependence of the line shape of the dark resonance when the dressing laser frequency is tuned in the range of the $12d[1/2]_1$ Rydberg state, on the detuning of the probe laser from the two-photon resonance of the $5p^6\,{}^1\mathrm{S}_0$–$5p^5\,6p[1/2]_0$ – transition in xenon. The line-profile is symmetric for exact two-photon resonance (frame (b)) and becomes asymmetric, when the probe laser is slightly tuned to higher (see frame (a), probe laser detuned +142 MHz from two-photon resonance) or lower frequencies (see frame (c), probe laser detuned −124 MHz from two-photon resonance).

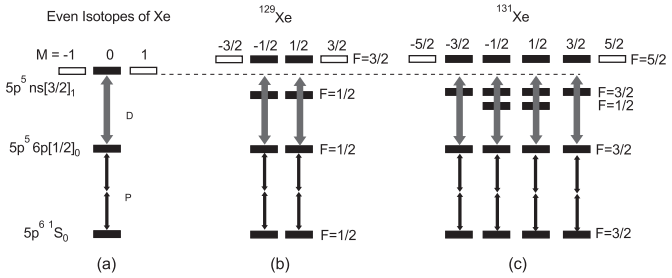

Fig. 6. Detailed coupling scheme for the even and the most prominent odd xenon isotopes including hyperfine structure.

Hyperfine splitting of several energy levels in xenon has been studied experimentally [24]. The magnetic dipole constant A and the electric quadrupole constants B were derived from these data. For different low lying energy levels of ^{129}Xe, the constant A is typically about a few GHz. The ratio $R = A_{129}/A_{131} = -0.2964$ between the constants A for ^{129}Xe and ^{131}Xe is determined by magnetic moments and spins of the respective nuclei. The electric quadrupole constant B of the relevant energy levels of ^{131}Xe does not exceed 100 MHz.

To the best of our knowledge values for the constants A and B for $5p^5ns[J_C]_1$ or $5p^5nd[J_C]_1$ Rydberg states studied in this paper are not available from the literature.

The detailed level scheme is shown in Figure 6 for different xenon isotopes, taking hyperfine structure into account. For even isotopes (52.5% of the xenon atoms) the coupling scheme is equivalent to a single three-level ladder system (see Fig. 6a). For ^{129}Xe (26.4%) each of the two magnetic sublevel of the intermediate state $5p^56p[1/2]_0$ is radiatively connected to both HFS components of the Rydberg state. Here we have two independent, but identical sets of coupled states, labeled by either $M_F = +1/2$ or $M_F = -1/2$. The coupling scheme for ^{131}Xe is more complicated. A fraction of 50% of these atoms (10.55% of all atoms) is in the $M = \pm 3/2$ state. For these atoms the coupling scheme is comparable to ^{129}Xe, *i.e.* the upper level is a doublet. The other fraction of 50% of the atoms is in the state $M = \pm 1/2$. For these atoms the intermediate level is coupled to a triplet of hyperfine components (see Fig. 6c). Here we have four independent subsets of levels. Each of the two subsets labeled by $M_F = -1/2$ and $M_F = +1/2$ or $M_F = -3/2$ and $M_F = +3/2$ are identical.

The consequences of the splitting of the target state for the shape of a dark resonances will be discussed next. The naive approach of simply adding two (or three) line profiles does not explain the observed line profiles of the $ns[3/2]_1$ resonances, which show both complete suppression of ionization as well as an enhancement in the center of the structure (see Fig. 4). Therefore a detailed analyses is required.

We consider first the simplest case of a dark resonance, involving only one upper level (Fig. 6a). The well known Hamiltonian for a ladder-type three-level scheme in rotating wave approximation reads [1]

$$\mathsf{H} = \frac{1}{2}\begin{bmatrix} 2\Delta_\mathrm{P} & \Omega_\mathrm{P} & 0 \\ \Omega_\mathrm{P} & -\mathrm{i}\gamma_2 & \Omega_\mathrm{D} \\ 0 & \Omega_\mathrm{D} & -2\Delta_\mathrm{D} - \mathrm{i}\gamma_3 \end{bmatrix} \tag{2}$$

where Ω_P is the effective two-photon Rabi frequency for the probe pulse, Ω_D is the Rabi frequency for the dressing laser pulse; $\Delta_\mathrm{P} = 2\omega_\mathrm{P} - \omega_{12}$ is the detuning of the probe laser frequency ω_P from two-photon resonance; $\Delta_\mathrm{D} = \omega_\mathrm{D} - \omega_{23}$ is the detuning of the dressing laser frequency ω_D from the resonance frequency for the transition between the intermediate state $|2\rangle$ and the target state $|3\rangle$; γ_2 and γ_3 are the ionization rates of the states $|2\rangle$ and $|3\rangle$ related to the probe and dressing laser fields.

The ionization signals S_2 and S_3 from states $|2\rangle$ and $|3\rangle$ are given by

$$S_i = \int_{-\infty}^{+\infty} |c_j(t)|^2 \gamma_j(t)\,\mathrm{d}t,\ (j = 2, 3). \tag{3}$$

For small probe laser intensity the ionization probability is small, *i.e.* $S_i \ll 1$ and neglect γ_i in the Hamiltonian (2). For a qualitative analysis of the dark resonances we determine the mean population of each of the states $|2\rangle$ and $|3\rangle$ during the interaction with the laser pulses as a function of the detuning Δ_D.

It is convenient to use a dressed state approach, in which the two dressed states $|+\rangle$ and $|-\rangle$, separated by the Autler-Townes splitting [1], are considered (instead of the two bare states $|2\rangle$ and $|3\rangle$ coupled by the strong dressing field). The two-level Hamiltonian is

$$\mathsf{H}' = \frac{1}{2}\begin{bmatrix} 0 & \Omega_\mathrm{D} \\ \Omega_\mathrm{D} & -2\Delta_\mathrm{D} \end{bmatrix}. \tag{4}$$

The dressed states are

$$|+\rangle = \cos\theta\,|3\rangle + \sin\theta\,|2\rangle \tag{5}$$

$$|-\rangle = -\sin\theta\,|3\rangle + \cos\theta\,|2\rangle \tag{6}$$

with the mixing angle θ given by

$$\tan 2\theta = \frac{\Omega_\mathrm{D}}{\Delta_\mathrm{D}}\,. \tag{7}$$

For slowly changing dressing laser intensity and with $\Omega_\mathrm{D}^{\max}\tau_\mathrm{D} \gg 1$ (with $\Omega_\mathrm{D}^{\max}$ as the peak value of $\Omega_\mathrm{D}(t)$ and τ_D is the dressing laser pulse duration), *i.e.* strong dressing laser induced coupling, nondiabatic coupling between dressed states is negligible small and the three state $(|1\rangle, |+\rangle, |-\rangle)$ dressed Hamiltonian reads

$$\mathsf{H} = \frac{1}{2}\begin{bmatrix} 2\Delta_\mathrm{P} & \Omega_\mathrm{P}^{(-)} & \Omega_\mathrm{P}^{(+)} \\ \Omega_\mathrm{P}^{(-)*} & 2\epsilon_- & 0 \\ \Omega_\mathrm{P}^{(+)*} & 0 & 2\epsilon_+ \end{bmatrix} \tag{8}$$

where

$$\epsilon_\pm = \frac{1}{2}\left[-\Delta_\mathrm{D} \pm \sqrt{\Delta_\mathrm{D}^2 + \Omega_\mathrm{D}^2}\right]. \tag{9}$$

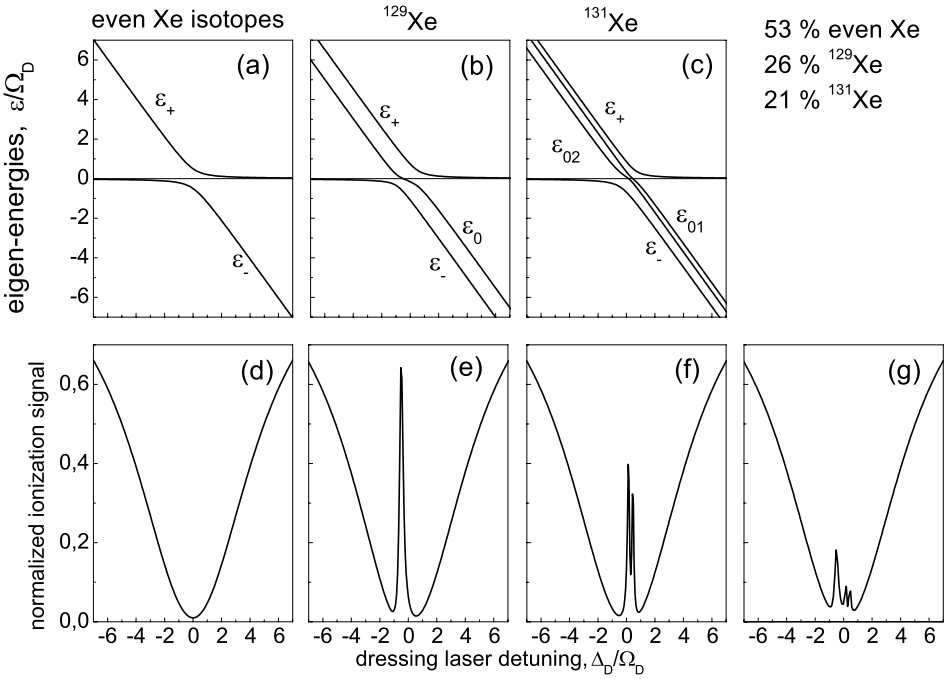

Fig. 7. Dressed energies (a, b, c) and ionization signal (d, e, f) for different isotopes of xenon plotted *versus* the dressing laser detuning $\Delta_{\rm D}$. The Rabi frequency in the simulation was chosen to be $\Omega_{\rm D} = A$ and the decay rate $\gamma = 0.1A$ in units of the magnetic dipole constant A, which determines the hyperfine splitting. The dark resonances for odd xenon isotopes clearly reveal a double-dip structure, as it is observed in the experiment (see Fig. 4). Frame (g) shows the line profile of the dark resonance, expected for the sum of the contributions from odd and even isotopes of xenon, weighted for their natural abundance (*i.e.* 53% even isotopes, 26% ^{129}Xe and 21% ^{131}Xe isotopes). The simulation presented in frame (g) confirms the experimental observation (see Fig. 4).

Dressed Rabi frequencies $\Omega_{\rm P}^{(+)} = (\sin\theta)\Omega_{\rm P}$ and $\Omega_{\rm P}^{(-)} = (\cos\theta)\Omega_{\rm P}$ describe the coupling of the ground state $|1\rangle$ with the dressed states $|+\rangle$ and $|-\rangle$. Figure 7a shows the eigenenergies as a function of the dressing laser detuning $\Delta_{\rm D}$, normalized to $\Omega_{\rm D}$, for exact resonance of the probe laser $\Delta_{\rm P} = 0$. The probe laser frequency is detuned from both dressed states if $|\Delta_{\rm D}| < \Omega_{\rm D}$. Excitation of both states is small, if the spectral width $\Delta\nu = 1/\tau_{\rm p}$ of the probe laser is much smaller than $\Omega_{\rm D}$. In this case the amplitude $c_2(t)$ of the bare state $|2\rangle$ during the interaction is found from the solution of the Schrödinger equation with the Hamiltonian (8). It is given by

$$c_2(t) = -1/2\left[\frac{\sin^2\theta}{\epsilon_+} + \frac{\cos^2\theta}{\epsilon_-}\right]\Omega_{\rm P}(t). \qquad (10)$$

Moreover, for exact resonance $\Delta_{\rm D} = 0$ (see Eqs. (7) and (10), respectively), resulting in $c_2(t) = 0$, we have $\theta = \pi/4$ and $\epsilon_+ = -\epsilon_- = \Omega_{\rm D}/2$, leading to the cancellation of the excitation probability of state $|2\rangle$ and thus the ionization signal S_2. Therefore the bare state $|2\rangle$ remains empty. Ionization from state $|3\rangle$ is not cancelled. However the signal S_3 is small due to the condition $\Omega_{\rm D}\tau_{\rm p} \gg 1$. When the detuning $|\Delta_{\rm D}|$ increases, the transition frequency to one of the dressed states gets closer to resonance with the probe laser frequency and the ionization probability increases. The dark resonance line shape *i.e.* the dependence of the ionization signal on detuning $\Delta_{\rm D}$ calculated in the stationary case for small probe laser intensity (for details see appendix) is shown in Figure 7d.

For ^{129}Xe the upper levels of the transitions driven by the dressing laser is composed of *two* hyperfine structure states. The effect of a hyperfine structure doublet on electromagnetically induced transparency is closely related to coherent population trapping described here. It has been previously investigated theoretically and experimentally by Hui Xia *et al.* [25]. The authors show that in the presence of a hyperfine doublet, EIT may be observed, if the laser frequencies are appropriately chosen. In our work, we analyze the observed lineprofils depending on detunings from the hyperfine levels aiming at spectroscopic applications.

Using angular momentum coefficients for the coupling of M_F states linear polarization by the light fields, the Hamiltonian of the four level system (see Fig. 6b) reads

$$\mathsf{H} = \frac{1}{2}\begin{bmatrix} 2\Delta_{\rm P} & \Omega_{\rm P} & 0 & 0 \\ \Omega_{\rm P} & 0 & \sqrt{1/3}\Omega_{\rm D} & \sqrt{2/3}\Omega_{\rm D} \\ 0 & \sqrt{1/3}\Omega_{\rm D} & -2\Delta_{\rm D} - 2A & 0 \\ 0 & \sqrt{2/3}\Omega_{\rm D} & 0 & -2\Delta_{\rm D} + A \end{bmatrix}. \qquad (11)$$

Here the detuning $\Delta_{\rm D}$ is defined with respect to the centre of gravity of the hyperfine doublet. Therefore the detuning

is defined as in Figure 7a. The dressed Hamiltonian reads

$$\mathsf{H} = \frac{1}{2}\begin{bmatrix} 2\Delta_{\mathrm{P}} & \Omega_{\mathrm{P}}^{(-)} & \Omega_{\mathrm{P}}^{(0)} & \Omega_{\mathrm{P}}^{(+)} \\ \Omega_{\mathrm{P}}^{(-)*} & \epsilon_+ & 0 & 0 \\ \Omega_{\mathrm{P}}^{(0))*} & 0 & \epsilon_0 & 0 \\ \Omega_{\mathrm{P}}^{(+)*} & 0 & 0 & \epsilon_- \end{bmatrix} \tag{12}$$

where $\Omega_{\mathrm{P}}^{(i)}$ $(i = \pm, 0)$ is the coupling of the ground state with the dressed state $|i\rangle$. The Rabi frequencies depend on the admixture $c_2^{(i)}$ to the bare state $|2\rangle$ in the respective dressed state $|i\rangle = c_2^{(i)}|2\rangle + c_3^{(i)}|3\rangle + c_4^{(i)}|4\rangle$. The coefficients $c_k^{(i)}$ are determined by Ω_{D} and Δ_{D}. The dependence of the eigenenergies ϵ_i on the detuning Δ_{D} is shown in Figure 7b for $\Omega_{\mathrm{D}} = A$. For small Δ_{D}, there is a "bright" resonance when the probe frequency is in resonance with the transition frequency to the dressed state $|0\rangle$. Thus, instead of two independent dark resonances, which may be expected for small dressing laser intensity ($\Omega_{\mathrm{D}} \ll A$), a narrow ionization enhancement is observed near the center of the broad dark resonance, if Ω_{D} is comparable to A. The width of this resonance is determined by the spectral width of the probe pulse or by the rate γ of other relaxation processes. Figure 7e shows the dark resonance shape calculated for the stationary case using equation (A.6). The dark resonance has the same shape as in the absence of hyperfine splitting, except for the central narrow peak.

The intensity of the narrow central peak is determined by the admixture $c_2^{(0)}$ to the bare state $|2\rangle$ in the dressed state $|0\rangle$. For the stationary case, *e.g.*, the ionization signal $S_{\max}$ at the central peak normalized to the signal S_0 in the absence of the dressing laser (or for large detunings $\Delta_{\mathrm{D}} \gg \Omega_{\mathrm{D}}$) can be obtained from equation (A.6). For small $\gamma \ll \Omega_{\mathrm{D}}, A$ it reads

$$S_{\max}/S_0 = \frac{2A^2}{2A^2 + \Omega_{\mathrm{D}}^2}\,. \tag{13}$$

Thus, the narrow peak near the centre of the dark resonance exists if $\gamma \ll \Omega_{\mathrm{D}} \leq A$. For Rabi frequencies much larger than the hyperfine splitting the latter becomes irrelevant and the situation as shown in Figures 7a and 7d is recovered. Because the strength of the coupling of state $|2\rangle$ with the various HFS components is different (see Eq. (11)) the narrow peak is shifted to the weaker component. For $\gamma \ll \Omega_{\mathrm{D}}$ this shift $\Delta_{\mathrm{D\,max}}$ is determined by the zero of the denominator of (A.6) for $\gamma = 0$ and reads

$$\Delta_{\mathrm{D\,max}} = -A/2. \tag{14}$$

In the case of a triplet upper state, as in ^{131}Xe a similar analysis along the same lines reveals *two* narrow peaks near the center of the dark resonances for $\gamma \ll \Omega_{\mathrm{D}} \leq A$. These peaks mirror the resonances with the two dressed states (see Fig. 7c). The shape of the dark resonance calculated for the stationary case in the assumption for a hyperfine splitting of ^{131}Xe with $A_{131} = -0.2964A$ and $B_{131} = 0$ is shown in Figure 7f. The overall shape of the dark resonance is the same as in the absence of hyperfine structure, but two narrow peaks appear in the center. The relative amplitudes of these peaks and their frequency positions depend on the relative strength of the coupling between the excited states and on the magnitude of the hyperfine splitting. For the stationary case they can be obtained from equation (A.6) using proper dressing laser Rabi frequencies and HFS intervals. For the case of small $\gamma \ll \Omega_{\mathrm{D}}, |A_{131}|$ the shift of the first resonance from the centre of the gravity is given by $\Delta_{\mathrm{D\,max}}^{(1)} = -A_{131}/2 = 0.1482A$ and the relative amplitude by

$$S_{\max}^{(1)}/S_0 = \frac{8A_{131}^2}{8A_{131}^2 + \Omega_{\mathrm{D}}^2}\,. \tag{15}$$

The second resonance is shifted to $\Delta_{\mathrm{D\,max}}^{(2)} = -3/2A_{131}$ and has the amplitude

$$S_{\max}^{(2)}/S_0 = \frac{6A_{131}^2}{6A_{131}^2 + \Omega_{\mathrm{D}}^2}\,. \tag{16}$$

In the experiment with natural xenon abundance the shape of dark resonances is the weighted sum of all three cases which should results in the broad dark resonance with three narrow peaks near the centre (see Fig. 7g). Within the limits of the resolution in our experiments we do not resolve the three narrow peaks, when the dressing laser couples the *ns*-Rydberg states to the intermediate state. However comparison of the simulation (see Fig. 7g) with the experimental data for *ns*-Rydberg states (see Fig. 4) shows excellent agreement both with regard to the magnitude of the bright resonance as well as its position slightly off-center from the minimum of the dark resonance. For the *nd*-Rydberg in xenon the hyperfine splitting is much smaller. Therefore the amplitudes of the peaks are very small. They cannot be observed in our experiment.

Obviously, the bright resonance for *odd* isotopes near the center of the dark resonance, which is observed for *all* isotopes, can be used to deplete the abundance of *odd* isotopes in a natural mixture.

3.3 Dark resonances induced by spectrally broad radiation

A more detailed theoretical analysis [12,23] of the interaction of an atomic or molecular three-level system with two coherent radiation fields yields a condition for the minimal Rabi frequency needed for (nearly complete) population trapping. This condition demands that the dressing Rabi frequency has to be much larger *than the rate of change* of the probe Rabi frequency throughout the interaction, *i.e.*

$$\left|\frac{\mathrm{d}}{\mathrm{d}t}(\Omega_{\mathrm{P}}(t)/\Omega_{\mathrm{D}}(t))\right| \ll \Omega_{\mathrm{D}}(t). \tag{17}$$

Because in the experiment the probe Rabi frequency is provided by a weak two-photon transition, while the dressing Rabi frequency is due to a strong one-photon coupling, and the pulse width of the dressing laser pulse is longer

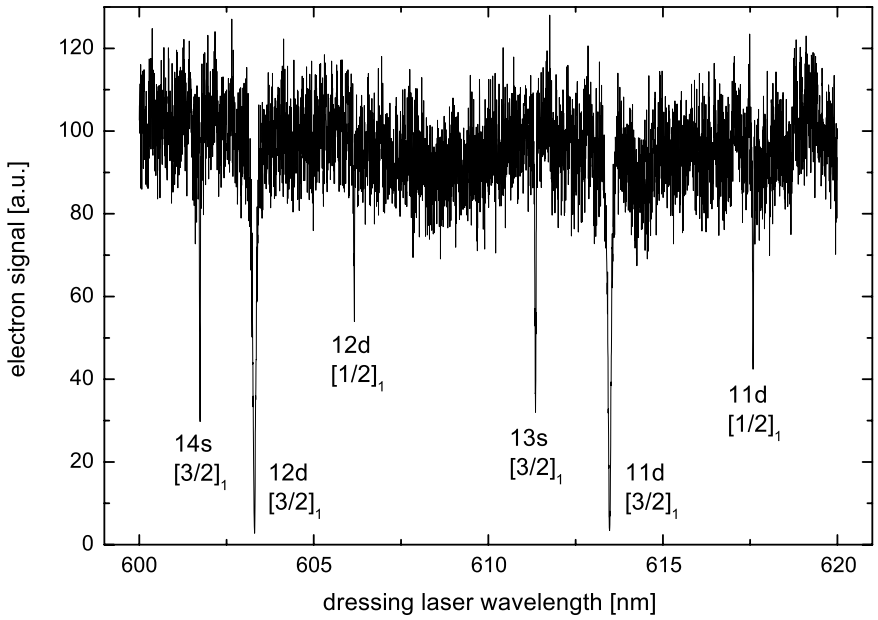

Fig. 8. Dark resonance spectrum, obtained with a multi-mode excimer-pumped dye laser-system. The coupling scheme is the same as shown in Figure 1. The lasers provided peak intensities of approximately 20 MW/cm^2 for the probe and 30 MW/cm^2 for the dressing pulse. The depth of most resonances clearly exceeds the value of 50%, expected for incoherent excitation, the strong $nd[3/2]_1$ resonances show nearly complete suppression of ionization.

than that of the probe pulse, the condition for the preparation of a dark state is well fulfilled. Fluctuations in the temporal profile of the probe laser pulse may be compensated by increasing the dressing Rabi frequency and/or by decreasing the probe Rabi frequency.

In the same way, phase fluctuations in the laser fields, which usually interfere with the dynamics of coherent excitation, may be overcome by coupling strength. An example of a coupling scheme for which the dynamics are insensitive to phase fluctuations is the so-called *incoherent interference control* (IIC) scheme [10]. Kuhn *et al.* [14] showed that detrimental effects of phase fluctuations may be compensated by an increase in laser intensities in order to permit efficient coherent population transfer by STIRAP. Kofman [13] investigated the effect of amplitude-phase-fluctuating radiation fields on EIT and found, that *significant* transparency may be induced even with light fields of poor coherence properties. We note, that the requirements for EIT in optically dense media are stronger than for the implementation of the dark resonances discussed here.

Therefore we expect pronounced dark resonances even when the laser pulses are not derived from a laser-system, which yields transform limited radiation (lacking phase fluctuations), but from a rather broadband excimer-laser pumped laser-system.

In fact the data shown in Figure 8 demonstrate that dark resonances are observable with a broadband laser-system. The excitation scheme is the same as shown in Figure 1. The laser pulse width was about 15 ns (FWHM of the intensity). The bandwidth $\Delta\nu = 6$ GHz exceeded the transform-limit by two orders of magnitude. Nevertheless the depth of most resonances clearly exceeds 50%, the value, expected to be the limit for dips caused by incoherent excitation. Due to stronger transition moments, the dark resonances are more pronounced when the dressing laser couples $nd[3/2]_1$ states to the intermediate level. In fact, the suppression of ionization approaches 100%.

The bright resonance in the center of the dark resonances, as observed for narrow-band excitation (see Fig. 4), can not be resolved in this setup, even when the intermediate level is coupled to ns Rydberg states.

4 Conclusion

We have observed pronounced population trapping in resonantly enhanced multi-photon ionization, when the intermediate state is coupled to a highly excited Rydberg state of xenon by a strong radiation field. The laser intensities which were necessary to induce substantial population trapping were of the order of several MW/cm^2 for a laser-system with nearly transform-limited bandwidth, but typically two orders of magnitude larger when a broadband laser-system was used. The depth of the ionization dips clearly exceeded the value of 50% expected for incoherent interaction. We have furthermore resolved the hyperfine structure in the ns-Rydberg state and and explained the consequence of that structure on the shape of the dark resonance, taking the natural abundance of xenon isotopes into account.

The authors like to thank H. Hotop, University of Kaiserslautern and B.W. Shore for valuable discussion on the manuscript. This work was supported by the European Union

Research under contract number HPRN-CT-1999-00129. Support by the Deutsche Forschungsgemeinschaft, the German-Israeli Foundation (1-644-118.5/1999) and the NATO-scientific affairs division (CRG 1507-826991) as well as by INTAS (99-00019) is also acknowledged.

Appendix

Here, the lineshape of the dark resonances is derived for the stationary case and for small probe laser intensity. The interaction of an atom with the probe and dressing lasers, assuming constant amplitudes, is given in the rotating wave approximation by the Hamiltonian

$$\mathsf{H} = \frac{1}{2}\begin{bmatrix} 2\Delta_\mathrm{P} & \Omega_\mathrm{P} & & & \\ \Omega_\mathrm{P} & & \Omega_\mathrm{D3} & \Omega_\mathrm{D4} & \Omega_\mathrm{D5} \\ & \Omega_\mathrm{D3} & -2\Delta_\mathrm{D1} & & \\ & \Omega_\mathrm{D4} & & -2\Delta_\mathrm{D2} & \\ & \Omega_\mathrm{D5} & & & -2\Delta_\mathrm{D3} \end{bmatrix} \quad \text{(A.1)}$$

where Δ_P is the two-photon detuning of the probe laser, $\Delta_{\mathrm{D}i}$ is the detuning of the dressing laser carrier frequency from the resonance with the upper state i, *i.e.* $\Delta_\mathrm{D3} = \Delta_\mathrm{D1} - \omega_{43}$, $\Delta_\mathrm{D4} = \Delta_\mathrm{D1} - \omega_{43} - \omega_{54}$, with ω_{ij} the frequency interval between states i and j. The Hamiltonian (A.1) includes all possible cases of HFS of Xe: for even isotopes of Xe the Rabi frequencies are $\Omega_\mathrm{D3} = \Omega_\mathrm{D}$, $\Omega_\mathrm{D4} = \Omega_\mathrm{D5} = 0$; for ^{129}Xe $\Omega_\mathrm{D3} = \sqrt{1/3}\Omega_\mathrm{D}$; $\Omega_\mathrm{D4} = \sqrt{2/3}\Omega_\mathrm{D}$, $\Omega_\mathrm{D5} = 0$ and $\omega_{43} = 3A/2$; for ^{131}Xe $\Omega_\mathrm{D3} = \sqrt{1/3}\Omega_\mathrm{D}$; $\Omega_\mathrm{D4} = \sqrt{1/15}\Omega_\mathrm{D}$ and $\Omega_\mathrm{D5} = \sqrt{3/5}\Omega_\mathrm{D}$, with $\omega_{54} = 5A_{131}/2 + 5B/4$, $\omega_{43} = 3A_{131}/2 - 9B_{131}/4$.

The master equation for the density matrix reads [1]

$$\frac{\partial}{\partial t}\rho = \frac{\mathrm{i}}{\hbar}\left[\mathsf{H}\rho\right] + \dot{\rho}_\mathrm{relax}. \quad \text{(A.2)}$$

In the case of a weak probe laser the diagonal elements of the density matrix describing the population of atomic states are $\rho_{11} = 1$ and $\rho_{ii} = 0$ $(i \neq 1)$. Furthermore, the off-diagonal density matrix elements ρ_{2j} $(j = 3, 4, 5)$ are neglected. Assuming the same relaxation rate γ for all matrix elements, the damping of the off-diagonal density matrix elements are described in simplest approximation by $(\dot{\rho}_\mathrm{relax})_{ij} = -\gamma\rho_{ij}$. This approach is appropriate to describe our experimental data, if relaxation is mainly due to finite interaction time, while relaxation due to spontaneous emission is negligibly small.

With these assumptions one obtains a system of four linear equations for the nonzero off-diagonal matrix elements ρ_{12} and ρ_{1j} $(j = 3, 4, 5)$

$$\frac{\mathrm{d}}{\mathrm{d}t}\rho_{12} + \left[\gamma + \mathrm{i}\Delta_\mathrm{P}\right]\rho_{12} = \frac{\mathrm{i}}{2}\Omega_\mathrm{P} + \frac{\mathrm{i}}{2}\sum_{j=3,4,5}\Omega_{\mathrm{D}j}\rho_{1j}, \quad \text{(A.3)}$$

$$\frac{\mathrm{d}}{\mathrm{d}t}\rho_{1j} + \left[\gamma + \mathrm{i}\left(\Delta_\mathrm{P} + \Delta_{\mathrm{D}j}\right)\right]\rho_{1j} = \frac{\mathrm{i}}{2}\Omega_{\mathrm{D}j}\rho_{12}. \quad \text{(A.4)}$$

In the stationary case $\dot{\rho} = 0$ the coherence ρ_{12} created between states 1 and 2 is given by

$$\rho_{12} = \frac{\frac{\mathrm{i}}{2}\Omega_\mathrm{P}}{\gamma + \mathrm{i}\Delta_\mathrm{P} + \frac{1}{4}\sum_{j=3,4,5}\frac{\Omega_{\mathrm{D}j}^2}{[\gamma + \mathrm{i}(\Delta_\mathrm{P} + \Delta_{\mathrm{D}j})]}}. \quad \text{(A.5)}$$

The power absorption of the probe field is proportional to $\mathrm{Re}(\rho_{12}\Omega_\mathrm{P}^*)$. Thus, the absorption coefficient $\varkappa$ for the probe field reads

$$\varkappa = \varkappa_0\,\mathrm{Re}\left[\frac{\gamma}{\gamma + \mathrm{i}\Delta_\mathrm{P} + \frac{1}{4}\sum_{j=3,4,5}\frac{\Omega_{\mathrm{D}j}^2}{[\gamma + \mathrm{i}(\Delta_\mathrm{P} + \Delta_{\mathrm{D}j})]}}\right] \quad \text{(A.6)}$$

where $\varkappa_0$ is the absorption coefficient for the probe field in the absence of the dressing laser. The stationary ionization rate from level 2 is proportional to the population of this level and therefore to $\varkappa$. Thus, the lineshape of a dark resonance is described by the expression derived in equation (A.6).

References

1. B.W. Shore, *The Theory of Coherent Atomic Excitation* (Wiley, New York, 1990).
2. L. Allen, J.H. Eberly, *Optical Resonances and Two-Level Atoms* (Wiley, New York, 1974).
3. K. Bergmann, H. Theuer, B.W. Shore, Rev. Mod. Phys. **70**, 1003 (1998).
4. T. Rickes, L.P. Yatsenko, S. Steuerwald, T. Halfmann, B.W. Shore, N.V. Vitanov, K. Bergmann, J. Chem. Phys. **113**, 534 (2000).
5. S. Harris, Phys. Today **50**, 36 (1997).
6. J.P. Marangos, J. Mod. Opt. **45**, 471 (1998).
7. E. Arimondo, Prog. Opt. **35**, 259 (1996).
8. P. Knight, M.A. Lauder, B.J. Dalton, Phys. Rep. **190**, 1 (1990).
9. M.H.R. Hutchinson, K.M.M. Ness, Phys. Rev. Lett. **60**, 105 (1988); X. Tang, A. L'Huillier, P. Lambropoulos, M.H.R. Hutchinson, K.M.M. Ness, *ibid.* **62**, 111 (1989); Y.L. Shao, D. Charalambidis, C. Fotakis, J. Zhang, P. Lambropoulos, *ibid.* **67**, 3669 (1991); S. Cavalieri, F.S. Pavone, M. Matera, *ibid.* **67**, 3673 (1991); S. Cavalieri, M. Matera, F.S. Cavone, J. Zhang, P. Lambropoulos, T. Nakajima, Phys. Rev. A **47**, 4219 (1993); O. Faucher, Y.L. Shao, D. Charalambidis, C. Fotakis, *ibid.* **50**, 641 (1994); S. Cavalieri, R. Eramo, L. Fini, J. Phys. B **28**, 1793 (1995); R. Eramo, S. Cavalieri, L. Fini, M. Matera, L.F. Di Mauro, J. Phys. B **30**, 3789 (1997); A. Shnitman, I. Sofer, I. Golub, A. Yogev, M. Shapiro, Z. Chen, P. Brumer, Phys. Rev. Lett. **76**, 2886 (1996); T. Halfmann, L.P. Yatsenko, M. Shapiro, B.W. Shore, K. Bergmann, Phys. Rev. A **58**, R46 (1998); L.P. Yatsenko, T. Halfmann, B.W. Shore, K. Bergmann, Phys. Rev. A **59**, 2926 (1999).
10. M. Shapiro, P. Brumer, Int. Rev. Phys. Chem. **13**, 187 (1994).
11. R. Sussmann, R. Neuhauser, N.J. Neusser, J. Chem. Phys. **100**, 4784 (1994); R. Neuhauser, R. Sussmann, H.J. Neusser, Phys. Rev. Lett. **74**, 3141 (1995); R. Sussmann, R. Neuhauser, H.J. Neusser, J. Chem. Phys. **103**, 3315 (1995).

12. T. Halfmann, K. Bergmann, J. Chem. Phys. **104**, 7068 (1996).
13. A.G. Kofman, Phys. Rev. A **56**, 2280 (1997).
14. A. Kuhn, G.W. Coulston, G.Z. He, S. Schiemann, K. Bergmann, W.S. Warren, J. Chem. Phys. **96**, 4215 (1992).
15. *Molecular Dynamics and Spectroscopy by Stimulated Emission Pumping*, edited by H.L. Dai, R.W. Field (World Scientific, Singapore, 1995).
16. G.Z. Zhang, D.W. Tokaryk, B.P. Stoicheff, K. Hakuta, Phys. Rev. A **56**, 813 (1997).
17. C.J. Latimer, Cont. Phys. **20**, 631 (1979).
18. K. Böhmer, T. Halfmann, L.P. Yatsenko, B.W. Shore, K. Bergmann, Phys. Rev. A, to be published.
19. L.P. Yatsenko, S. Guerin, T. Halfmann, K. Böhmer, B.W. Shore, K. Bergmann, Phys. Rev. A **58**, 4683 (1998).
20. S. Guerin, L.P. Yatsenko, T. Halfmann, K. Böhmer, B.W. Shore, K. Bergmann, Phys. Rev. A **58**, 4691 (1998).
21. P. Labastie, F. Biraben, E. Giacobino, J. Phys. B **15**, 2595 (1982).
22. K. Yoshino, D. E. Freeman, J. Opt. Soc. Am. B **2**, 1268 (1985).
23. T. Halfmann, *Dark Resonances and Laser Induced Continuum Structure: Experiments in SO2 and metastable helium*, Ph.D. thesis, University of Kaiserslautern, Kaiserslautern, 1998.
24. D.A. Jackson, M.C. Coulombe, Proc. R. Soc. Lond. A **327**, 137 (1972); D.A. Jackson, M.C. Coulombe, Proc. R. Soc. Lond. A **335**,127 (1973); W. Fischer, H. Hühnermann, G. Kromer, H.J. Schäfer, Z. Phys. **270**, 113 (1974); W.L. Faust, M.N. McDermott, Phys. Rev. **123**, 198 (1961); W. Borchers, E. Arnold, W. Neu, R. Neugart, K. Wendt, G. Ulm, Phys. Lett. B **216**, 7 (1989); H. Geisen, T. Krumpelmann, D. Neuschäfer, Ch. Öttinger, Phys. Lett. A **130**, 299 (1988); G. D'Amico, G. Pesce, A. Sasso, Phys. Rev. A **60**, 4409 (1999).
25. Hui Xia, S.J. Sharpe, A.J. Merriam; S. E. Harris, Phys. Rev. A **56**, 3362 (1998); Hui Xia, A.J. Merriam, S.J. Sharpe, G.Y. Yin, S.E. Harris Phys. Rev. A **59**, R3190 (1999).